Thermal Equation of State of Fe_3S and Implications for Sulfur in Earth's Core

Christopher T. Seagle[1], Andrew J. Campbell[2], Dion L. Heinz[1, 3], Guoyin Shen[4, *], and Vitali B. Prakapenka[4]

[1]*Department of the Geophysical Sciences, the University of Chicago, Chicago, IL 60637*

[2]*Department of Geology, University of Maryland, College Park, MD 20742*

[3]*The James Franck Institute, the University of Chicago, Chicago, IL 60637*

[4]*The Consortium for Advanced Radiation Sources, the University of Chicago, Chicago, IL 60637*

[*]*Currently at High Pressure Collaborative Access Team, Advanced Photon Source, Argonne National Laboratory, Argonne, IL 60439*

Abstract

Iron (Fe) and coexisting Fe_3S were studied simultaneously using synchrotron x-ray diffraction and a laser heated diamond anvil cell (DAC). The thermal equation of state (EOS) of Fe_3S was investigated up to pressures of 80 GPa and temperatures of 2500 K. Fitting a 3rd order Birch-Murnaghan EOS to the room temperature data yielded bulk modulus K_0 =156(7) GPa, and pressure derivative K'_0=3.8(3) calibrated against NaCl in the B2 structure. The room temperature data was also calibrated against the EOS of hcp-Fe for comparison and aid in the determination of the thermal pressure contribution of Fe_3S. This fit yielded bulk modulus K_0 =113(9) GPa, and pressure derivative K'_0=5.2(6). The thermal pressure contribution of Fe_3S was assumed to be of the form $\Delta P_{thermal}=\alpha K_T \Delta T$, where αK_T is constant. The best fit to the data yielded αK_T=0.011(2) GPa/K. Iron and Fe_3S coexisted in the high pressure, high temperature experiments, and a density relationship between Fe and Fe_3S was found to be linear and independent of temperature. Extrapolation of the data to the core-mantle boundary (CMB), using an assumed temperature of 3500 K at the CMB, a 2% volume change associated with melting, and applying a small adjustment to account for the nickel content of the core indicates that 14.7(11) wt. % sulfur is adequate to resolve the density deficit of the outer core.

Introduction

The properties of iron under high pressures and temperatures are of great importance to the geophysics of terrestrial planet interiors. It has been known for some time that Earth's core is composed mainly of iron (Fe) and a fraction of light elements [*Birch*, 1952]. Therefore, knowing the properties of iron compounds and alloys at core conditions enhances our understanding of Earth and planetary evolution. Sulfur is one of the light elements suspected to be important in Earth's core, because of its solar abundance and the ease with which it forms compounds with Fe. Other possibilities include O, C, Si, and H [*Poirier*, 1994]. The only direct samples we have of planetary cores, the iron meteorites, contain abundant evidence of sulfur, in the form of sulfide inclusions and/or trace element fractionations that reveal the presence of a cogenetic sulfide melt.

At pressures above 21 GPa, Fe_3S is the stable sulfide phase in the Fe-FeS system at compositions more iron rich then 16.1 wt. % S; this phase was discovered and characterized by *Fei et al.* [2000]. The density relationship between Fe and Fe_3S is of primary importance for estimating the amount of sulfur that can satisfy the observed density deficit in the outer core. The electronic environment surrounding sulfur in solid Fe_3S is probably very similar to the electronic environment that would be encountered in the core fluid if sulfur is the dominant light element. The Fe-FeS system exhibits eutectic behavior to at least 25 GPa and the eutectic composition was found to be 14.7 wt. % S at this pressure [*Li, et al.*, 2001]. If eutectic behavior persists to core pressures and the eutectic composition remains close to Fe_3S, then the structure of solid Fe_3S is likely to be close to the short range order of the liquid core, justifying the comparison of solid Fe plus

Fe_3S to the liquid outer core. Cosmochemical and seismological constraints, combined with high pressure experiments on iron sulfides, allow an evaluation of the sulfur content in Earth's core.

It has also been recognized that as much as 14.2 wt. % sulfur may be incorporated into the Martian core based on the compositions of the SNC-meteorites (Shergottites, Nakhlites, Chassigny) [*Dreibus and Wanke*, 1987]. Extensive work has been performed on stoichiometric iron sulfide (troilite) at pressures relevant to the Martian core [*Kavner, et al.*, 2001; *Urakawa, et al.*, 2004]: however, the sulfur content of troilite (36.5 wt. %) is significantly greater then that estimated to be in the Martian core and there are no indications of the Fe-Fe_3S system exhibiting complete solid solution behavior in the pressure range 21-80 GPa. Fe_3S has a sulfur content close to recent estimates of the Martian core based on numerical modeling [*Zharkov and Gudkova*, 2005]. The lack of seismic data from Mars makes it difficult to accurately model the interior structure. However, other constraints such as the moment of inertia and cosmochemical arguments do provide useful criteria to evaluate the sulfur content and size of the Martian core. The Martian core is likely in the liquid state based on its estimated composition, temperature and eutectic temperatures in the Fe-FeS system at high pressures [*Fei and Bertka*, 2005].

Fe_3S undergoes a magnetic collapse at 21 GPa [*Lin, et al.*, 2004]. It was proposed by those authors that a volume change may be associated with this transition, but a volume collapse is not evident from previous work [*Fei, et al.*, 2000]. Diffraction data indicating that a structural transition is associated with the magnetic transition has been reported in an abstract [*Shen, et al.*, 2003], in our data analysis we have assumed that no structural transition has taken place. An ab initio simulation of possible Fe_3S polymorphs

concluded that only the Fe_3P-type polymorph was stable along the 0 K isotherm [*Martin, et al.*, 2004].

In the present study, the lattice parameters of Fe and coexisting Fe_3S were measured simultaneously at high pressures and temperatures. The volume difference between the two phases was thereby measured to high precision, avoiding many of the uncertainties inherent in comparing equation of state data from separate studies. This approach, we argue, provides a more exact understanding of the density difference between iron and iron sulfide at high P, T conditions, and permits an improved examination of the density deficit of the outer core.

Experimental Procedure

Starting materials were mixtures of powdered Fe and iron sulfide (FeS), mechanically ground together for several hours. Two compositions were used in this study; the bulk composition of the sample mixture consisted of 5 or 15 wt. % S. The sample material was sandwiched between 5-15 μm thick layers of sodium chloride (NaCl). The diamond culets had a diameter of 250 μm for most of the experiments; 400 μm culets were used for some of the data below 40 GPa. The gasket material was stainless steel or Inconel. The gaskets were pre-indented to 40 μm, and 100 μm holes were drilled in the gasket to serve as the sample chamber.

Double sided laser heating experiments were preformed at Sector 13 of the Advanced Photon Source at Argonne National Laboratory [*Newville, et al.*, 1999; *Shen, et al.*, 2001]. The samples were heated using Nd:YLF lasers, focused to a spot size of ~30 μm [*Shen, et al.*, 2005]. Temperatures were measured from the central 5 μm of the laser

heated region using the spectroradiometric method with the grey-body assumption [*Heinz and Jeanloz*, 1987].

Monochromatic synchrotron radiation (λ=0.3344 Å) was used with angle dispersive detection. The x-ray beam was focused horizontally and vertically to a 5 x 7 μm (FWHM) spot using Kirkpatrick-Baez mirrors. The area of the sample probed by x-ray diffraction was therefore much smaller than the laser heated spot, and similar to the area measured spectroradiometrically, minimizing errors associated with radial temperature gradients in the laser-heated cell. Coalignment of the x-ray beam and the laser-heating/temperature measurement system was accomplished with the aid of x-ray induced fluorescence from the NaCl pressure medium, viewed through the temperature measurement portion of the optical system [*Shen, et al.*, 2005]. Diffraction patterns were collected on a MAR345 image plate detector. A CeO_2 standard was used to calibrate the sample-to-detector distance and the detector tilt. The diffraction image was converted to a linear diffraction pattern using FIT2D [*Hammersley, et al.*, 1996], and peak positions were determined using the peak fitting program PeakFit (Jandel Scientific Software).

After compression of each sample to high pressures, Fe_3S was formed by reaction between Fe and FeS upon laser heating, with excess Fe remaining. Fe_3S has tetragonal symmetry with space group $I\bar{4}$ and 8 formula units per unit cell [*Fei, et al.*, 2000; *Martin et al.*, 2004]. The Levenberg-Marquardt nonlinear fitting method was used to determine the unit cell parameters and the associated asymptotic standard error from indexed peaks. The most commonly used peaks entering the Fe_3S regressions are shown in Table 1 along with their d-spacings and corresponding lattice parameters determined from those peaks at a series of pressures.

The pressures assigned to room temperature diffraction patterns were calculated using the EOS of NaCl in the B2 structure [*Heinz and Jeanloz*, 1984]. A Mie-Grüneisen thermal EOS of hcp-Fe, with explicit vibrational and electronic contributions to the specific heat, was used to calculate the pressure in high temperature patterns. The full equation of state is of the form:

$P = P_{isotherm} + P_{thermal}$ where $P_{isotherm}$ is given by the 3rd order Birch-Murnaghan EOS and

$$P_{thermal} = \gamma\rho(E_{thermal} - E_0)$$

$$\gamma = \gamma_0 (\frac{\rho_0}{\rho})^q$$

$$E_{thermal} = \frac{9nRT}{(\Theta_T/T)^3} \int_0^{\Theta_T/T} \frac{\xi^3}{e^\xi - 1} d\xi + \frac{\beta_e}{2} (\frac{\rho_0}{\rho})^{\gamma_e} (T^2 - 300^2)$$

$$E_0 = \frac{9nR \times 300}{(\Theta_T/300)^3} \int_0^{\Theta_T/300} \frac{\xi^3}{e^\xi - 1} d\xi$$

$$\Theta_T = \Theta_0 e^{(\gamma_0 - \gamma)/q}$$

Where γ is the Grüneisen parameter, ρ is the specific mass, E is energy, $q = -\left(\frac{\partial \ln \gamma}{\partial \ln \rho}\right)$ is typically assumed to be constant, n is the number of atoms per formula unit, R is the gas constant, T is the temperature, β_e is the coefficient of the electronic specific heat, γ_e is the electronic Grüneisen parameter, Θ_T is the Debye temperature, and the subscript 0 refers to ambient conditions. The first term in the expression for $E_{thermal}$ is the Debye model of vibrational energy, and the second term is the electronic contribution as calculated by *Boness et al.* [1986]. In this study, we used the room temperature compression of hcp-Fe given by *Mao et al.* [1990], and a fit of the above equations to the data of *Mao et al.*

[1990] and *Brown et al.* [2000] was used to constrain γ_0 and q. The Debye temperature of hcp-Fe was estimated from the work of *Mao et al.* [2001]. Table 2 shows the parameters used for the thermal EOS of hcp-Fe.

Results

Fe_3S was synthesized and compressed from 22 to 80 GPa in a diamond anvil cell in a series of experiments. Figure 1 shows typical diffraction patterns collected in this study. The data used to determine the room temperature EOS of Fe_3S were all collected after laser heating the sample; the thermal relaxation of the sample and insulator during this heating reduces pressure gradients and improves the accuracy of the results. All data except the first point were calibrated to sodium chloride in the B2 structure [*Heinz and Jeanloz,* 1984]. The pressure of the first data point was calculated with the EOS of sodium chloride in the B1 structure [*Sato-Sorensen*, 1983]. A third order Birch-Murnaghan EOS was determined using a linear least squares regression on a normalized pressure, F, versus eulerian strain f [*Birch*, 1978]. The zero pressure volume of Fe_3S found by *Fei et al.* [2000], 377.0(2) $Å^3$, was used in the fitting procedure; the uncertainty on the ambient pressure volume of Fe_3S was propagated through the fitting procedure. The best fit of the room temperature compression curve yielded bulk modulus K_0 =156(7) GPa and pressure derivative K'_0=3.8(3) calibrated to sodium chloride. The number(s) in parentheses refers to the uncertainty in the last digit(s), for example 3.8(3) is equivalent to 3.8 ± 0.3 and 14.7(11) is 14.7 ± 1.1. The bulk modulus falls within error of the value found by *Fei et al.* [2000], 150 GPa with K'_0 fixed to 4. The compression curve agrees well with previous data (Figure 2) [*Fei, et al.*, 2000].

A room temperature EOS from our Fe_3S data was also calibrated against hcp-Fe [*Mao, et al.*, 1990], for comparison to the NaCl-based EOS and also to aid in the estimation of the thermal contribution to the pressure of Fe_3S. This fit yielded K_0 =113(9) GPa and first pressure derivative K'_0=5.2(6) for Fe_3S; these parameters were used in the determination of the thermal EOS of Fe_3S. The discrepancy of the fit parameters based on the hcp-Fe and NaCl B2 calibrations may indicate the need to reevaluate the EOS of hcp-Fe or NaCl B2. The use of the more recent NaCl B2 EOS [*Sata, et al.*, 2002] gives lower pressures for the same volume compared to the EOS of *Heinz and Jeanloz* [1984] and did not satisfactorily reproduce the Fe_3S compression curve of *Fei et al.* [2000]. The complete data set of the volumes of Fe, Fe_3S, and NaCl along with the calculated pressures and temperatures are tabulated in Table 3.

A structural transition associated with the magnetic transition has been reported in an abstract [*Shen, et al.,* 2003], our analysis of the data has assumed that no structural transition has taken place. Since no volume collapse is observed over the magnetic transition [*Fei, et al.,* 2003], and there is currently no knowledge of the temperature dependence of the transition, we assume that any possible volume effects of crossing the transition at higher pressures and temperatures can be ignored. The observed magnetic collapse is consistent with a high spin to low spin transition caused by ligand interactions with the crystal field. Little is known about the structure of liquid Fe_3S; however, if short range order is preserved in the transition from solid to liquid Fe_3S, then Fe_3S will likely remain in the low spin state because the crystal field effect is dominated by nearest neighbors.

The thermal EOS of hcp-Fe (Table 2) was used to determine the pressure of the Fe + Fe_3S sample during laser heating. In the sample geometry used in these experiments, Fe and Fe_3S were mechanically well mixed, so these 2 phases experienced the same P, T conditions. In contrast, NaCl was located adjacent to the anvils and acted as a thermal insulator, transparent to the heating laser; therefore it is not strictly appropriate to use NaCl as the high-T pressure standard. To establish a thermal EOS for Fe_3S, the thermal contribution to the pressure for Fe_3S was then calculated from $P_{thermal}(Fe_3S) = P(Fe, high\ T) - P(Fe_3S, room\ T)$, where $P(Fe_3S, room\ T)$ refers to the room temperature EOS of Fe_3S calibrated against hcp-Fe.

All but two of the data points used in these calculations had measured axial temperature gradients less than 100 K; the others were less then 140 K. The calculated thermal pressure is plotted against ΔT (=T-300 K) (Figure 3). The thermal contribution to the pressure of the sample was assumed to be of the form: $\Delta P_{thermal}=\alpha K_T \Delta T$ where αK_T=constant [*Anderson*, 1984]. More complicated expressions of the thermal pressure were found to be not justified by the data. The best fit to our high-P, T data for Fe_3S yielded αK_T=0.011(2) GPa/K.

Discussion

Previous studies on the effect of sulfur in the Martian core have based their results on the assumption that the density of an intermediate Fe-S composition could be calculated using a linear combination of the density of fcc-Fe and FeS at a given pressure [*Kavner, et al.*, 2001; *Urakawa, et al.*, 2004]. In order to evaluate the reliability of this assumption we calculate the density of an Fe-14 wt. % S liquid at 31 GPa and ~1600 K neglecting any volume change on melting. Under these conditions the density of an Fe-14

wt. % S liquid is 8.30(1) g/cc; we have taken the density of the liquid to be a linear combination of the measured densities of hcp-Fe and Fe_3S at 31(4) GPa and ~1600 K. The density of Fe-14 wt. % S calculated from a linear combination of the density of FeS (6.398 g/cc) determined from the EOS data from *Urakawa et al.* [2004], and the density of fcc-Fe (8.394 g/cc) [*Funamori, et al.*, 1996] under similar conditions is ~8.21 g/cc, very comparable to the density calculated using a linear combination of hcp-Fe and Fe_3S densities. The slight difference may be a result of the density difference between fcc-Fe and hcp-Fe. The true density of liquid Fe-S would provide a more exact treatment for Martian core calculations, however because this data is not currently available it is useful to know that consistent results can be obtained by using a linear combination of the density of Fe and the density of either Fe_3S or FeS.

The nature of the experiments carried out in this study allows a direct comparison of the specific volume of Fe and Fe_3S at simultaneous high pressure and temperature. The comparative density of Fe and Fe_3S follows a linear relationship at all pressures and temperatures included in this study (Figure 4). The relationship is shown with the figure. Note that this correlation between $\rho(Fe)$ and $\rho(Fe_3S)$ is independent of the pressure calibration. We believe the linear relationship is a coincidental balance of the thermoelastic properties of iron and Fe_3S. The extrapolated ambient pressure density of hcp-Fe at 300 K is 8.30 g/cc [*Mao, et al.*, 1990]. Plugging this value into the linear density relationship predicts the density of Fe_3S as ambient conditions to be 7.09(7) g/cc; the measured density of Fe_3S at ambient conditions, 7.033 g/cc [*Fei, et al.*, 2000], falls within the uncertainty of the predicted density, suggesting extrapolations to higher pressures are not presumptuous. A relationship such as this is of great value because the

precise EOS parameters must only be known for one of the phases in order to determine the density of the other at some P, T conditions. Figure 5 illustrates the ratio of molar volumes between Fe and Fe_3S as density is increased. This figure highlights the similarity in mean atomic volume between the two phases, especially at high compression. At low compression sulfur has the effect of increasing the average distance between atoms relative to pure iron, but at higher compression it may actually decrease the average volume per atom. Data at higher pressure is needed to conclude if this ratio continues to decrease with pressure or asymptotes to a constant. Above 50 GPa the density difference between the two phases can be attributed principally to the lower atomic mass of S, while at lower pressures the difference is also due to the increased volume per atom relative to Fe. This is particularly useful because if we wish to calculate the density of an Fe-S melt, it may be assumed that the average volume per atom does not change with composition at a given pressure.

At 25 GPa, *Li et al.* [2001] found limited solid solution behavior in the Fe-Fe_3S system with a maximum sulfur solubility of 0.8 wt. % S. In this analysis, we have assumed that if there is solubility at higher pressures it does not significantly affect the density of Fe. This assumption is justified by the results, which show very little difference in mean atomic volume between hcp-Fe and Fe_3S (Fig. 5).

At the highest pressures to which Fe-S phase relations have been studied experimentally in detail [*Li, et al.*, 2001], the stable sulfide on the Fe-rich side of the phase diagram is Fe_3S; therefore the density of this phase is the best proxy one can use to evaluate the effect of sulfur substitution for Fe at the conditions of the Earth's core assuming the average volume per atom is independent of possible solid solution behavior.

An estimate of the amount of sulfur required in Earth's outer core to resolve the density deficit can be made if we assume a temperature for the CMB and estimate the volume change associated with melting Fe and Fe_3S. We assume the temperature at the outermost core to lie between 2500 and 4500 K as reasonable values [*Boehler*, 1993; *Williams, et al.*, 1987], and use the thermal EOS of hcp-Fe presented earlier to calculate the density of iron under these conditions. The linear density relationship described above can then be employed to calculate the density of Fe_3S at CMB conditions. For example, solving the thermal EOS of hcp-Fe at 135.8 GPa and 3500 K gives the density of iron as 11.07 g/cc. Applying the linear density relationship described above gives the density of Fe_3S as 10.07(7) g/cc under these conditions; the uncertainty reported here is taken as the root mean square of the linear fit.

The S content of Fe_3S (16.1 wt %) is of the same order as the maximum S content permissible in the Earth's core [*Li and Fei*, 2003]. Therefore, we assume that the electronic environment surrounding S in Fe_3S is comparable to that of an Fe-S liquid of similar composition, to justify the comparison of outer core densities with a mixture of Fe_3S and hcp-Fe densities. Adjusting the volume of the mixture by 1 - 3% for the effect of melting [*Anderson and Isaak*, 2000; *Laio, et al.*, 2000] gives the density of the iron-iron sulfide melt. Comparing these densities to the Preliminary Earth Reference Model (PREM) (ρ(CMB)=9.90 g/cc), an estimation of the amount of sulfur needed to resolve the density deficit can be made [*Poirier*, 1994]. The result of this procedure is shown in Figure 6. The outcome of these calculations show that the S content that is compatible with PREM densities is a strong function of the assumed temperature of the outermost core, varying from 17.5(13) wt. % S at 2500 K to 10.3(8) wt. % S at 4500 K for a fixed

$\Delta V_{melting}$ of 2%. The uncertainty on the wt. % S is based solely on the root mean square of the linear density relation fit and was calculated using standard error propagation techniques. The addition of 6.4 wt. % Ni to the core [*McDonough*, 2003] increases the wt. % S adequate to resolve the density deficit by 0.55% at 2500 K and 0.48% at 4500 K for a fixed $\Delta V_{melting}$ of 2%. This correction for the presence of Ni falls within the uncertainty of the calculations, and is not included in Figure 6.

We note that the sulfur content inferred for the outer core in this way is very sensitive to the equation of state adopted for hcp-Fe, and uncertainty in the hcp-Fe equation of state is not reflected in our estimates of the S content of the outer core. Continued refinement of this EOS, using an array of developing technologies to improve its accuracy and precision, will be of great benefit. It should also be noted that there is no reason to suspect that there is only one light element present in Earth's core. The addition of other elements is expected to change the density relationship at high pressure. Finally, little is known about the melting behavior of Fe_3S at high pressure, particularly with regard to its ΔV.

The strategy employed in this study, that of simultaneously measuring the specific volume of iron and a candidate light element containing iron phase at high pressures and temperatures, provides a useful means for gauging the abundance of a particular light element that is required to satisfy the outer core density deficit assuming that there is no or limited solubility of the light element in iron. This method can be extended to ternary and quaternary systems which, combined with sound velocity measurements, may further constrain the composition of Earth's core.

Acknowledgements

We would like to thank James Devine and Wendy Mao for helping collect the data. We also thank two anonymous reviewers and the associate editor, Yingwei Fei, for helpful comments. This work was preformed at GeoSoilEnviro CARS (Sector 13), Advanced Photon Source (APS), Argonne National Laboratory. GeoSoilEnviro CARS is supported by the National Science Foundation – Earth Sciences (EAR – 0217473), Department of Energy – Geosciences (DE – FG02 – 94ER14466) and the State of Illinois. Use of the APS was supported by the U. S. Department of Energy, Basic Energy Sciences, Office of Science, under Contract No. W – 31 – 109 – Eng – 38. This work was supported by NSF grants EAR 0309486 (DLH) and EAR 0330591 (AJC).

References

Anderson, O. L. (1984), A universal thermal equation-of-state, *J. Geodyn.*, *1*, 185-214.

Anderson, O. L., and D. G. Isaak (2000), Calculated melting curves for phases of iron, *Am. Mineral.*, *85*, 376-385.

Birch, F. (1952), Elasticity and constitution of the Earth's interior, *J. Geophys. Res.*, *57*, 227-286.

Birch, F. (1978), Finite strain isotherm and velocities for single-crystal and polycrystalline NaCl at high-pressures and 300-degree-K, *J. Geophys. Res.*, *83*, 1257-1268.

Boehler, R. (1993), Temperatures in the Earth's core from melting-point measurements of iron at high static pressures, *Nature*, *363*, 534-536.

Boness, D. A., J. M. Brown, and A. K. McMahan (1986), The electronic thermodynamics of iron under Earth core conditions, *J. Phys. Earth*, *42*, 227-240.

Brown, J. M., J. N. Fritz, and R. S. Hixson (2000), Hugoniot data for iron, *J. Appl. Phys.*, *88*, 5496-5498.

Dreibus, G., and H. Wanke (1987), Volatiles on Earth and Mars - A comparison, *Icarus*, *71*, 225-240.

Fei, Y. W., and C. Bertka (2005), The interior of Mars, *Science*, *308*, 1120-1121.

Fei, Y. W., J. Li, C. M. Bertka, and C. T. Prewitt (2000), Structure type and bulk modulus of Fe_3S, a new iron-sulfur compound, *Am. Mineral.*, *85*, 1830-1833.

Funamori, N., T. Yagi, and T. Uchida (1996), High-pressure and high-temperature in situ x-ray diffraction study of iron to above 30 GPa using MA8-type apparatus, *Geophys. Res. Lett.*, *23*, 953-956.

Hammersley, A. P., S. O. Svensson, M. Hanfland, A. N. Fitch, and D. Hausermann (1996), Two-dimensional detector software: From real detector to idealised image or two-theta scan, *High Press. Res.*, *14*, 235-248.

Heinz, D. L., and R. Jeanloz (1984), Compression of the B2 high-pressure phase of NaCl, *Phys. Rev. B*, *30*, 6045-6050.

Heinz, D. L., and R. Jeanloz (1987), Measurement of the melting curve of $Mg_{0.9}Fe_{0.1}SiO_3$ at lower mantle conditions and its geophysical implications, *J. Geophys. Res.*, *92*, 11437-11444.

Kavner, A., T. S. Duffy, and G. Y. Shen (2001), Phase stability and density of FeS at high pressures and temperatures: implications for the interior structure of Mars, *Earth Planet. Sci. Lett.*, *185*, 25-33.

Laio, A., S. Bernard, G. L. Chiarotti, S. Scandolo, and E. Tosatti (2000), Physics of iron at Earth's core conditions, *Science*, *287*, 1027-1030.

Li, J., and Y. Fei (2003), Experimental Constraints on Core Composition, in *Treatise on Geochemistry*, vol. 2, edited by R. W. Carlson, pp. 521-546, Elsevier, New York.

Li, J., Y. Fei, H. K. Mao, K. Hirose, and S. R. Shieh (2001), Sulfur in the Earth's inner core, *Earth Planet. Sci. Lett.*, *193*, 509-514.

Lin, J. F., Y. W. Fei, W. Sturhahn, J. Y. Zhao, H. K. Mao, and R. J. Hemley (2004), Magnetic transition and sound velocities of Fe_3S at high pressure: implications for Earth and planetary cores, *Earth Planet. Sci. Lett.*, *226*, 33-40.

Mao, H. K., Y. Wu, L. C. Chen, J. F. Shu, and A. P. Jephcoat (1990), Static compression of iron to 300 GPa and $Fe_{0.8}Ni_{0.2}$ alloy to 260 GPa - implications for composition of the core, *J. Geophys. Res.*, *95*, 21737-21742.

Mao, H. K., J. Xu, V. V. Struzhkin, J. Shu, R. J. Hemley, W. Sturhahn, M. Y. Hu, E. E. Alp, L. Vocadlo, D. Alfe, G. D. Price, M. J. Gillan, M. Schwoerer-Bohning, D. Hausermann, P. Eng, G. Shen, H. Giefers, R. Lubbers, and G. Wortmann (2001), Phonon density of states of iron up to 153 gigapascals, *Science*, *292*, 914-916.

Martin, P., L. Vocadlo, D. Alfe, and G. D. Price (2004), An ab initio study of the relative stabilities and equations of state of Fe_3S polymorphs, *Mineralogical Magazine*, *68*, 813-817.

McDonough, W. F. (2003), Compositional Model for the Earth's Core, in *Treatise on Geochemistry*, vol. 2, edited by R. W. Carlson, pp. 547-568, Elsevier, New York.

Newville, M., S. Sutton, M. Rivers, and P. Eng (1999), Micro-beam x-ray absorption and fluorescence spectroscopies at GSECARS: APS beamline 131D, *J. Synchrotron Radiat.*, *6*, 353-355.

Poirier, J. P. (1994), Light-elements in the Earth's outer core - a critical review, *J. Phys. Earth*, *85*, 319-337.

Sata, N., G. Y. Shen, M. L. Rivers, and S. R. Sutton (2002), Pressure-volume equation of state of the high-pressure B2 phase of NaCl, *Phys. Rev. B*, *65*, 104114-1-104114-7.

Sato-Sorensen, Y. (1983), Phase-transitions and equations of state for the sodium-halides - NaF, NaCl, NaBr, and NaI, *J. Geophys. Res.*, *88*, 3543-3548.

Shen, G., M. L. Rivers, Y. B. Wang, and S. R. Sutton (2001), Laser heated diamond cell system at the Advanced Photon Source for in situ x-ray measurements at high pressure and temperature, *Rev. Sci. Instrum.*, *72*, 1273-1282.

Shen, G., J. Lin, Y. Fei, H. Mao, M. Hu, P. Chow (2003), Magnetic and structural transition in Fe_3S at high pressures, *Eos Trans. AGU*, 84(46), Fall Meet. Suppl., Abstract V31D-0961.

Shen, G., V. Prakapenka, P. Eng, M. Rivers, and S. Sutton (2005), Facilities for high-pressure research with the diamond anvil cell at GSECARS, *J. Synchrotron Radiat.*, *12*, 642-649.

Urakawa, S., K. Someya, H. Terasaki, T. Katsura, S. Yokoshi, K. I. Funakoshi, W. Utsumi, Y. Katayama, Y. I. Sueda, and T. Irifune (2004), Phase relationships and equations of state for FeS at high pressures and temperatures and implications for the internal structure of Mars, *J. Phys. Earth*, *143-44*, 469-479.

Williams, Q., R. Jeanloz, J. Bass, B. Svendsen, and T. J. Ahrens (1987), The melting curve of iron to 250 gigapascals - a constraint on the temperature at Earth's center, *Science*, *236*, 181-182.

Zharkov, V. N., and T. V. Gudkova (2005), Construction of Martian interior model, *Solar System Research*, *39*, 343-373.

Figure Captions

Figure 1. Typical diffraction patterns collected in this study with background subtracted. The patterns clearly show the coexistence of Fe and Fe_3S at simultaneous high pressure and temperature. Top pattern, P=79.4(19) GPa, T=2150 K; bottom pattern, after rapid quenching P=74.9(7) GPa, λ=0.3344 Å. Stars, NaCl B2 reflections; crosses, hcp-Fe reflections; tick marks, all Fe_3S reflections allowed by symmetry based on the lattice parameters *a*=8.306(6) Å and *c*=4.104(5) Å determined from the quenched pattern. The small peak at ~11.5 degrees in the high temperature pattern remains unidentified.

Figure 2. Fe_3S compression curve at T=300 K. Solid circle, this study; open square, *Fei et al.* [2000]; solid line, best fit to our data, K_0=156(7) GPa, K'_0=3.8(3).

Figure 3. Fe_3S thermal pressure. $P_{thermal}=\alpha K_T \Delta T$, where ΔT=(T-300 K). Thick solid line, best fit αK_T=0.011(2) GPa/K; thin solid lines, one sigma error.

Figure 4. Density comparison between Fe_3S and Fe. Open diamonds, data at high temperature; solid circles, data at room temperature; solid line, best fit to the data. The data follows a linear relationship independent of temperature. The best fit yielded $\rho(Fe_3S)=-1.832(g/cc)+1.075* \rho(Fe)$, with root mean square 0.069 g/cc.

Figure 5. Volume per atom of Fe_3S:Fe. Open diamonds, data at high temperature; solid circles, data at room temperature. Sulfur has the effect of decreasing the average volume per atom relative to pure iron above ~50 GPa.

Figure 6. Weight percent sulfur required to resolve the density deficit of the outer core as a function of the temperature at the core mantle boundary. Solid line, dV=1%; dashed line, dV=2%; dotted line, dV=3%. The relative uncertainty for a given

point is ~7.5% relative, based solely on the uncertainty of the density of Fe_3S. See the text for procedure of determining these curves.

Tables

Table 1. Most commonly observed Fe_3S peaks used in the data regression at T=300 K and corresponding lattice parameters *a* and *c*. The column headings are the pressure in GPa, the d-spacings and lattice parameters are in Å; hkl are the Miller indices. The data presented here are averages of several patterns collected at similar pressure.

(hkl)	0[a]	22.6(5)	34.4(6)	53.3(14)	60(2)	74.7(7)	79.9(4)
031	2.5273	2.4163	2.3935	-	2.3175	2.2998	2.2952
321	2.2108	2.1150	2.0961	2.0541	-	-	-
330	2.1560	-	2.0421	-	-	1.9658	-
112	2.1262	2.0319	2.0143	1.9773	1.9624	1.9384	1.9293
420	2.0449	-	1.9340	1.8955	1.8806	1.8593	-
202	2.0225	1.9312	-	1.8772	-	1.8504	1.8350
141	1.9891	1.9032	1.8819	1.8494	-	1.8116	1.8079
222	1.8478	1.7684	1.7505	1.7137	1.7025	1.6829	1.6775
510	1.7942	1.7205	1.7021	1.6663	-	1.6314	-
312	1.7782	1.6960	1.6848	1.6523	1.6367	1.6207	1.6127
501	1.6948	-	1.6045	-	1.5588	1.5455	1.5380
a	9.144(2)	8.761(6)	8.663(5)	8.491(6)	8.399(9)	8.326(7)	8.312(5)
c	4.509(2)	4.301(3)	4.268(4)	4.186(3)	4.155(5)	4.113(5)	4.087(2)

[a]Zero pressure data are from *Fei et al.* [2000].

Table 2. hcp-Fe EOS parameters used in this study

K_0 (GPa)[a]	164.8
K'_0[a]	5.33
V_0 (cc/mol)[a]	6.687
γ[b]	2.4
q[b]	1.2
β_e (kJ/g/K^2)[c]	9.10x10^8
γ_e (kJ/g/K^2)[c]	1.34
Θ_0 (K)[d]	380

[a][*Mao, et al.*, 1990]
[b][*Brown, et al.*, 2000]
[c][*Boness, et al.*, 1986]
[d]Estimated from Figure 4 [*Mao, et al.*, 2001]

Table 3. Summary of P-V-T data set. The pressure calculated from the volume of NaCl is not reported in the high temperature patterns because it was used as the insulating medium and did not experience the same temperature as the sample material. The volume of NaCl is the volume of the B2 phase unless otherwise noted.

File	Temperature (K)[a]	V Fe_3S (Å^3)	V Fe (Å^3)	V NaCl (Å^3)	P Fe (GPa)	P NaCl (GPa)
Aug04_028	300	332.1(5)	20.12(3)	28.97(6)	22.9(17)	27.3(4)
Nov04_181	300	330.3(5)	20.25(12)	122.7(4)[b]	21(5)	22.6(5)
Aug04_123	300	321.3(12)	19.82(2)	27.68(4)	27.3(14)	33.7(2)
Nov04_203	300	321.2(9)	19.75(1)	27.46(5)	28.4(14)	34.9(4)
Nov04_206	300	319.9(4)	19.72(3)	27.54(15)	28.9(18)	34.5(10)
Nov04_332	300	306.3(5)	18.94(2)	25.14(11)	42.5(18)	50.5(10)
Nov04_336	300	305.0(5)	18.96(11)	24.9(3)	42(5)	53(3)
Nov04_226	300	303.7(11)	18.87(14)	24.80(12)	44(6)	53.3(13)
Nov04_218	300	302.7(6)	18.886(4)	24.83(17)	43.5(16)	53.0(18)
Nov04_228	300	302.3(6)	19.02(14)	24.82(4)	41(6)	53.2(4)
Nov04_222	300	301.3(6)	19.13(1)	24.76(18)	38.9(15)	54(3)
Nov04_224	300	301.1(4)	18.790(4)	24.75(8)	45.4(16)	53.7(9)
Nov04_220	300	300.7(6)	18.812(3)	24.82(12)	45.0(16)	53.2(13)
Aug04_165	300	294.3(4)	18.41(1)	24.04(14)	53.7(18)	60.2(13)
Nov04_410	300	285.5(11)	17.88(10)	22.75(7)	67(5)	74.0(8)
Nov04_390	300	284.8(5)	17.88(5)	22.61(4)	67(3)	75.7(5)
Nov04_402	300	284.5(3)	17.90(4)	22.72(6)	66(3)	74.4(7)
Nov04_408	300	283.8(8)	17.86(8)	22.71(6)	67(4)	74.6(7)
Nov03_03_037	300	283.3(11)	17.67(3)	22.28(3)	73(3)	79.9(4)
Nov04_180	1585/1583	335.7(4)	20.46(9)	123.2(12)[b]	31(4)	
Nov04_325	1748/1778	311.8(5)	19.06(1)	25.17(4)	54.6(16)	
Nov04_329	1920/1892	311.3(10)	19.07(3)	25.24(7)	56(2)	
Nov04_327	1817/1826	310.4(4)	18.98(4)	25.20(4)	57(2)	
Nov04_321	1687/1671	310.3(7)	19.09(5)	25.15(3)	53(3)	
Nov04_323	1694/1726	310.2(7)	19.08(2)	25.16(2)	53.6(16)	
Nov04_335	2036/2123	309.9(9)	18.96(5)	25.10(3)	60(3)	
Nov04_217	1617/1673	308.7(6)	19.08(5)	25.0(2)	53(3)	
Nov04_221	1808/1818	307.2(9)	19.0481(4)	24.98(10)	55.3(15)	
Nov04_223	1879/1878	307.0(7)	19.20(3)	25.20(12)	53.4(18)	
Nov04_227	1891/1941	306.6(5)	19.16(6)	25.3(3)	54(3)	
Nov04_219	1766/1763	306.3(4)	19.12(8)	25.0(2)	54(4)	
Nov04_225	1810/1836	306.0(5)	19.14(5)	25.3(2)	54(3)	
Nov04_215	1478/1558	304.7(3)	19.05(8)	24.95(9)	52(4)	
Nov04_393	1860/1724	289.0(2)	18.13(2)	22.80(3)	75(2)	
Nov04_395	1913/1987	288.8(3)	18.176(8)	22.80(6)	75.3(19)	
Nov04_391	1740/1685	288.6(2)	18.01(6)	22.78(13)	77(3)	
Nov04_401	2522/2481	287.8(2)	18.15(3)	22.93(10)	82(2)	
Nov04_397	1993/2105	287.6(6)	18.12(1)	22.86(4)	78(2)	
Nov04_387	1498/1471	287.4(6)	18.03(3)	22.69(2)	74(2)	
Nov04_389	1696/1612	287.1(5)	18.00(2)	22.72(4)	76(2)	
Nov04_399	2152/2167	287.1(5)	18.102(2)	22.85(3)	79.4(19)	

[a]High temperature patterns are labeled as temperature measured upstream/downstream of the sample relative to the x-ray beam.

[b]Volume of NaCl B1.

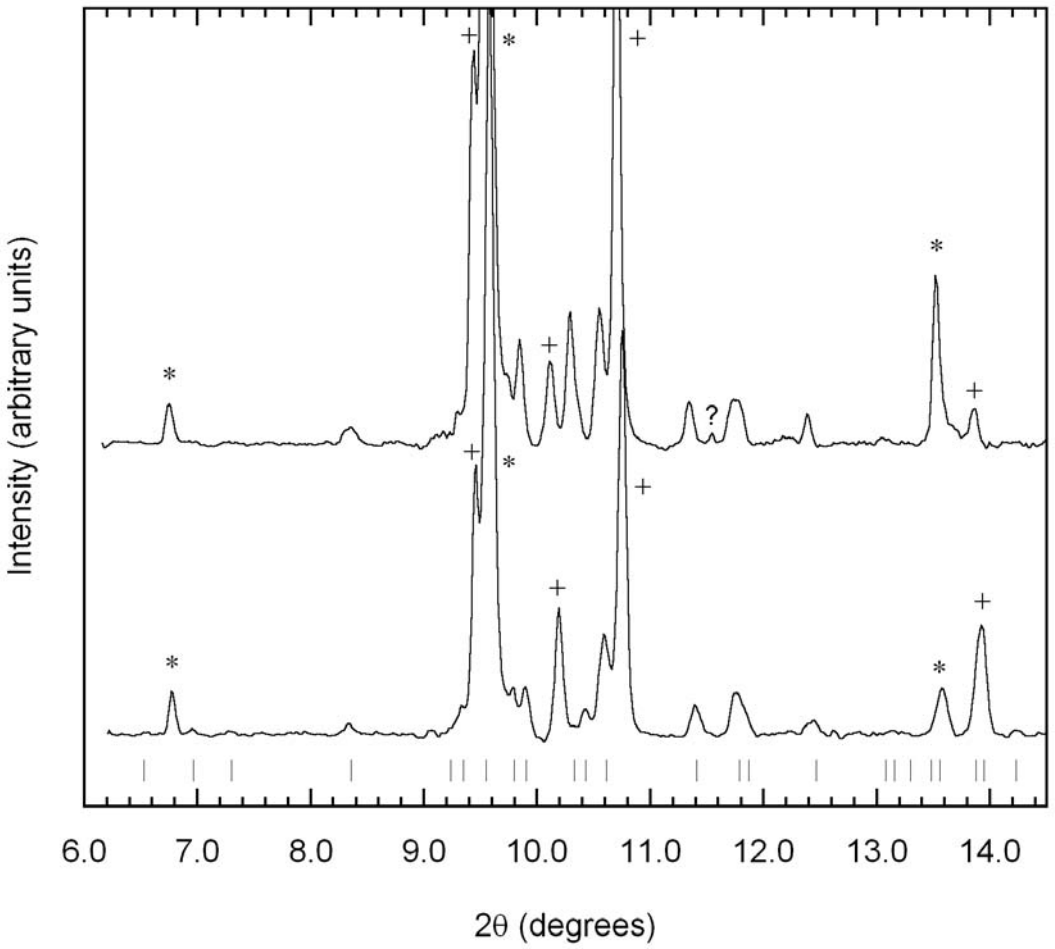

Figure 1. Typical diffraction patterns collected in this study with background subtracted. The patterns clearly show the coexistence of Fe and Fe_3S at simultaneous high pressure and temperature. Top pattern, P=79.4(19) GPa, T=2150 K; bottom pattern, after rapid quenching P=74.9(7) GPa, λ=0.3344 Å. Stars, NaCl B2 reflections; crosses, hcp-Fe reflections; tick marks, all Fe_3S reflections allowed by symmetry based on the lattice parameters *a*=8.306(6) Å and *c*=4.104(5) Å determined from the quenched pattern. The small peak at ~11.5 degrees in the high temperature pattern remains unidentified.

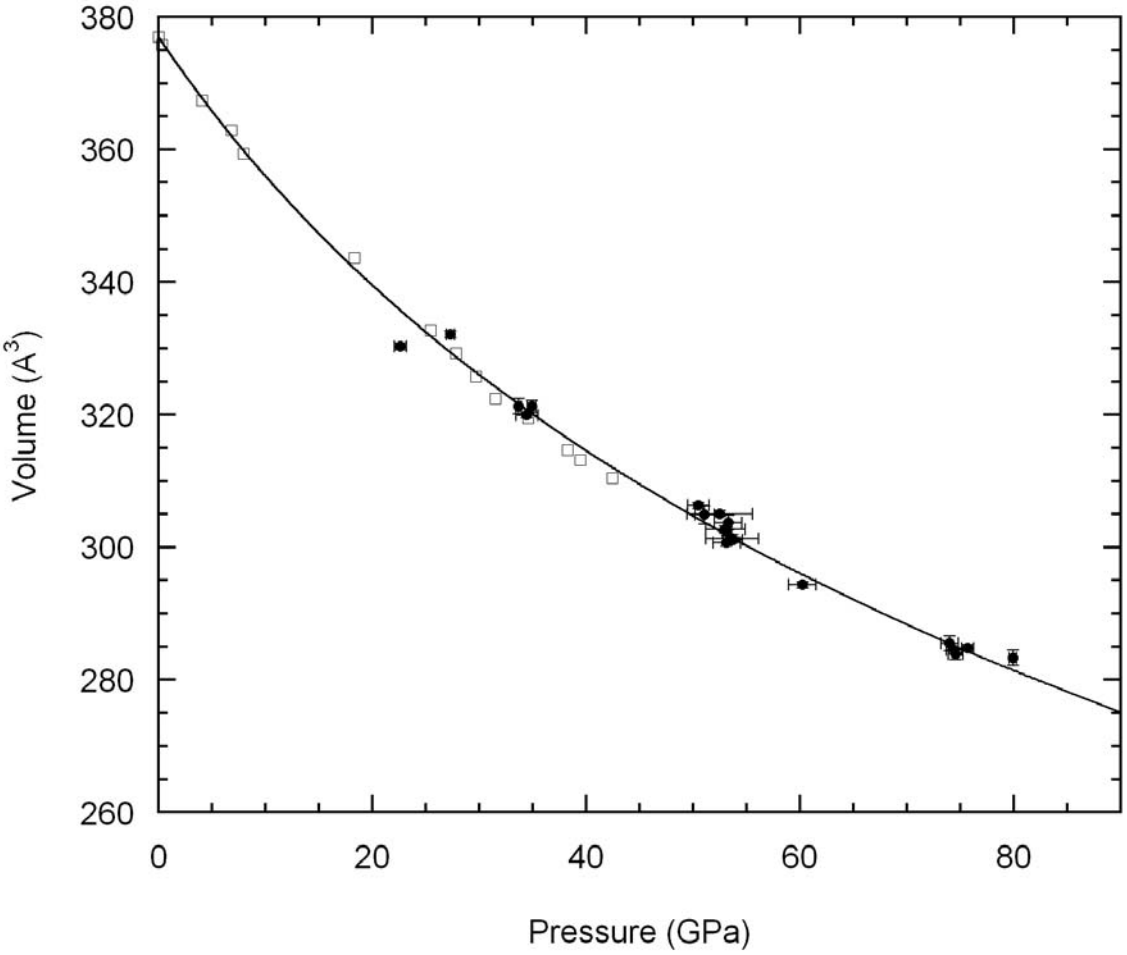

Figure 2. Fe_3S compression curve at T=300 K. Solid circle, this study; open square, *Fei et al.* [2000]; solid line, best fit to our data, K_0=156(7) GPa, K'_0=3.8(3).

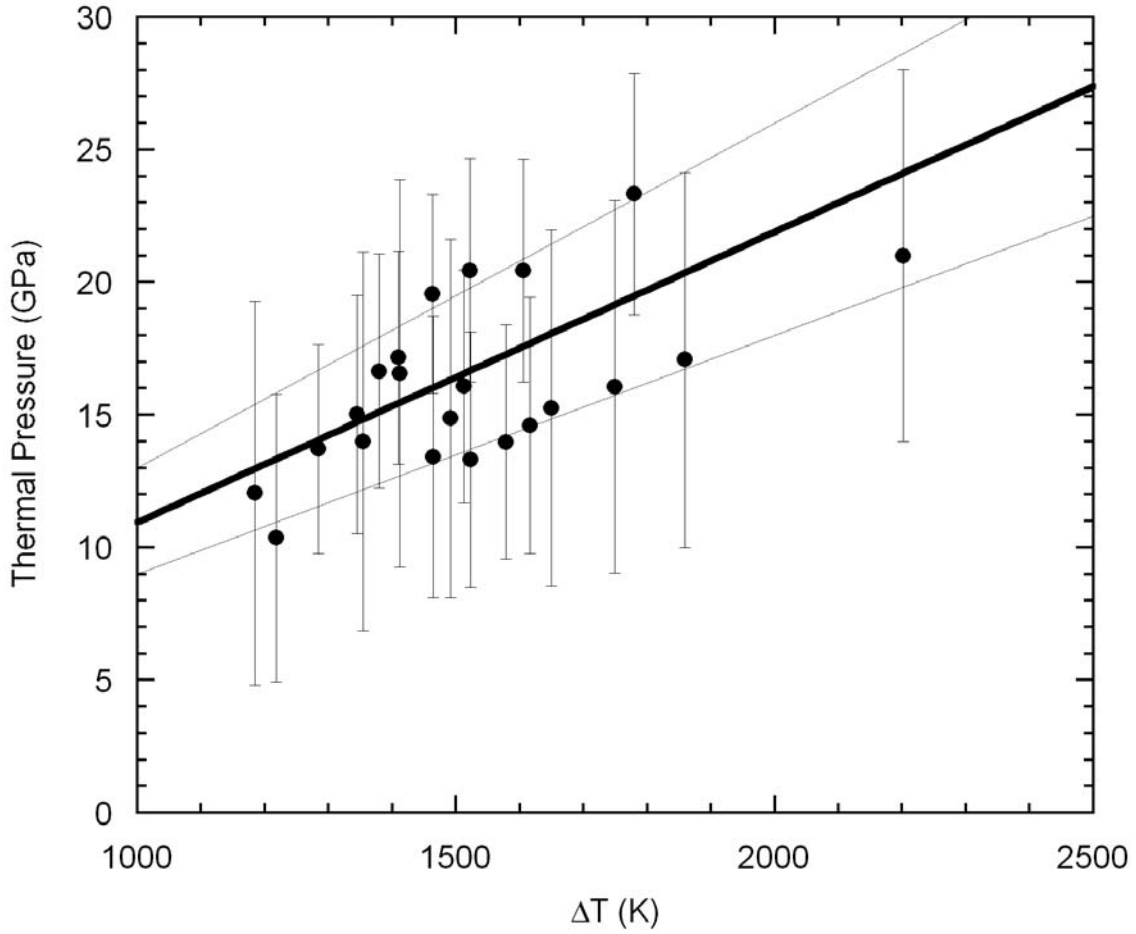

Figure 3. Fe_3S thermal pressure. $P_{thermal}=\alpha K_T \Delta T$, where $\Delta T=(T-300\ K)$. Thick solid line, best fit $\alpha K_T=0.011(2)$ GPa/K; thin solid lines, one sigma error.

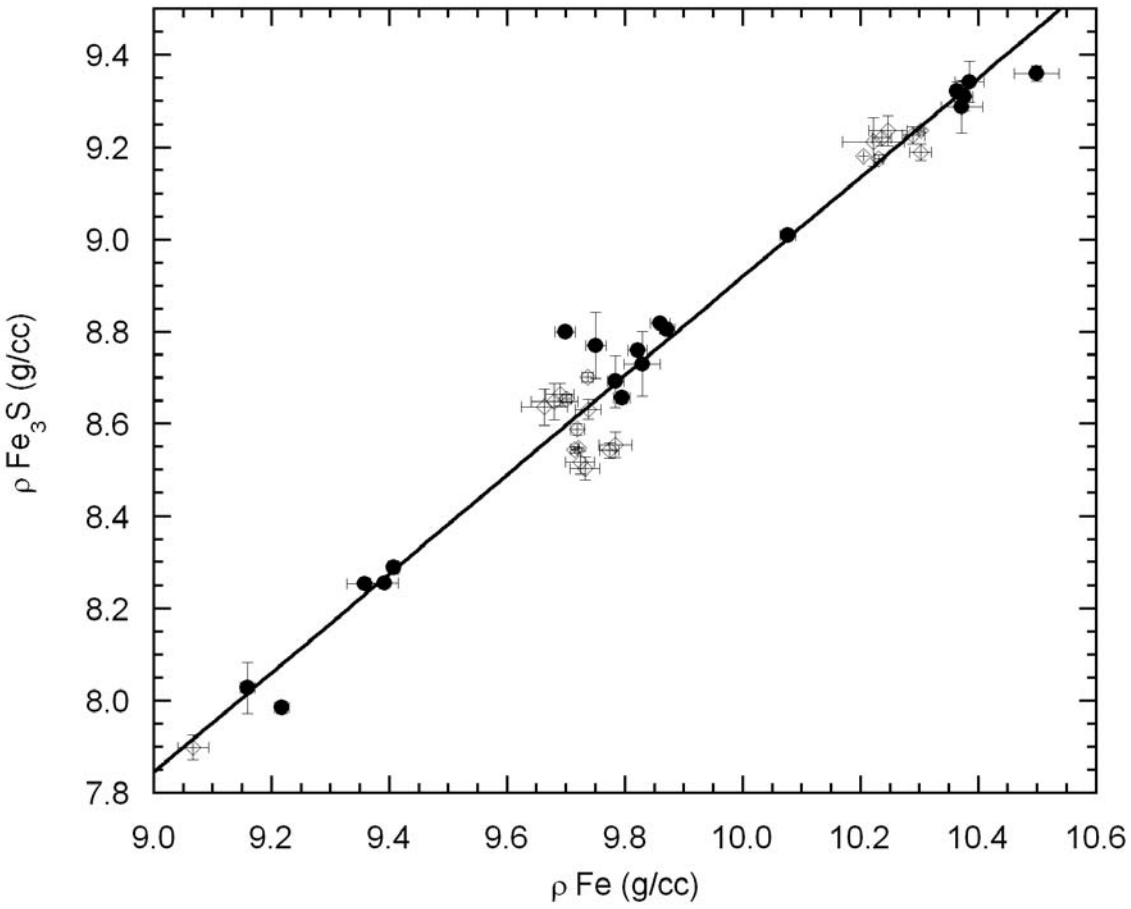

Figure 4. Density comparison between Fe_3S and Fe. Open diamonds, data at high temperature; solid circles, data at room temperature; solid line, best fit to the data. The data follows a linear relationship independent of temperature. The best fit yielded $\rho(Fe_3S)=-1.832(g/cc)+1.075* \rho(Fe)$, with root mean square 0.069 g/cc.

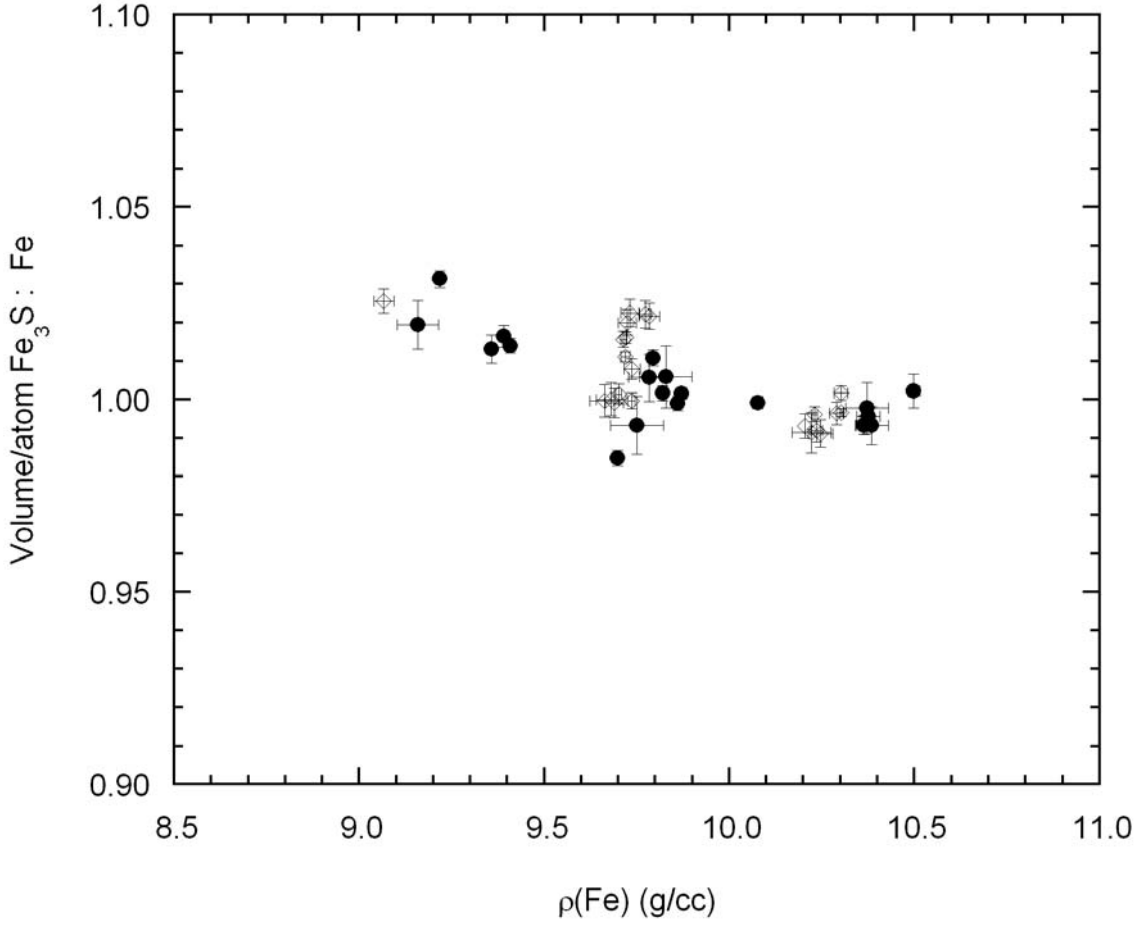

Figure 5. Volume per atom of Fe_3S:Fe. Open diamonds, data at high temperature; solid circles, data at room temperature. Sulfur has the effect of decreasing the average volume per atom relative to pure iron above ~50 GPa.

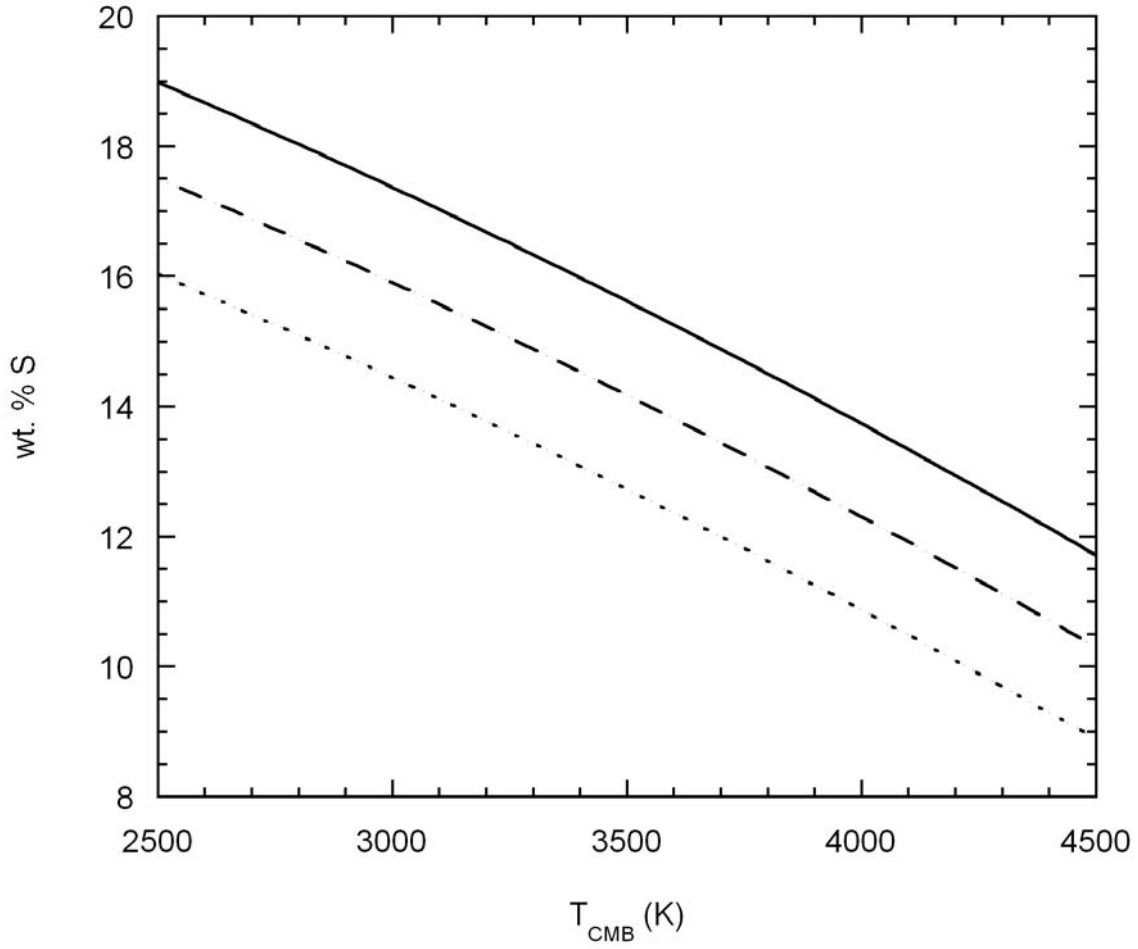

Figure 6. Weight percent sulfur required to resolve the density deficit of the outer core as a function of the temperature at the core mantle boundary. Solid line, dV=1%; dashed line, dV=2%; dotted line, dV=3%. The relative uncertainty for a given point is ~7.5% relative, based solely on the uncertainty of the density of Fe_3S. See the text for procedure of determining these curves.